Particle & Particle Systems Characterization

www.particle-journal.com

Nuclear Uptake of Gold Nanoparticles Deduced Using Dual-Angle X-Ray Fluorescence Mapping

*Aaron McCulloch, Lindsey Bennie, Jonathan A. Coulter, Helen O. McCarthy, Brendan Dromey, David R. Grimes, Paul Quinn, Balder Villagomez-Bernabe, and Frederick Currell**

Studies into the cell nucleus' incorporation of gold nanoparticles (AuNPs) are often limited by ambiguities arising from conventional imaging techniques. Indeed, it is suggested that to date there is no unambiguous imaging evidence for such uptake in whole cells, particularly at the single nanoparticle level. This shortcoming in understanding exists despite the nucleus being the most important subcellular compartment in eukaryotes and gold being the most commonly used metal nanoparticle in medical applications. Here, dual-angle X-ray flouresence is used to show individually resolved nanoparticles within the cell nucleus, finding them to be well separated and 79% of the intranuclear population to be monodispersed. These findings have important implications for nanomedicine, illustrated here through a specific exemplar of the predicted enhancement of radiation effects arising from the observed AuNPs, finding intranuclear dose enhancements spanning nearly five orders of magnitude.

1. Introduction

Nanomedicine is an area undergoing enormous growth in part due to the potential for engineering at the cellular level. Nanoparticles comprised of a metal core, typically surrounded by functionalizing groups, are a major tool in the nanomedicine revolution.

Predominant among these nanoparticles are gold nanoparticles (AuNPs).[1] While a lot is known about uptake of AuNPs into cells and some of the cellular compartments,[2–4] far less is known about their uptake into the most important cellular compartment—the nucleus.

As the hub for gene expression the nucleus is responsible for governing all cellular processes, making it a key target in nanomedicine. Widely reported in literature are numerous benefits of successful AuNP uptake into the nucleus such as improved radiotherapy treatment by exploiting AuNPs' dose enhancing properties,[5] novel regimes to combat illnesses such as HIV through the use of NP-mediated drug or gene delivery,[6,7] and the ability to cause disruption to the nuclear structure itself.[8,9]

To achieve nuclear uptake many studies use liposomal delivery or a cell penetrating peptide (CPP) coating on the AuNP,[10–12] thereby ensuring free dispersion within the cytosol and circumnavigating the traditional route of entry into the cell via endosome. A nuclear localization sequence (NLS) tagged onto the AuNP is often then used to ensure nuclear targeting once inside the cell.

However, it has been suggested that within such studies there is no unambiguous imaging evidence for uptake into the cell nucleus.[13] Fluorescence microscopy is highly useful as a fast, easy, and low-cost method to image multiple organelles at once. Many studies have imaged cells treated with fluorescently tagged-AuNPs in this manner and reported evidence of cellular uptake or intracellular localization.[6,14,15] Yet, they fail to account for the fact that single microscope projections cannot be used to infer information regarding the 3D position of the objects observed. Use of confocal fluorescence microscopy in studies provides greater spatial information due to the restricted z-field provided.[9,16] However, this remains an indirect method of observing AuNPs, with the marker being imaged rather than the nanoparticle, creating anomalous results should detachment occur. Transmission electron microscopy (TEM) is a powerful technique, providing nanometer resolution and a restricted z-field, which has been used to study the localization of AuNPs.[11,17] Yet, the excessive sample preparation required for TEM can be detrimental to the biological relevance of studies, ultrathin

A. McCulloch, Dr. B. Dromey, Dr. D. R. Grimes, Dr. B. Villagomez-Bernabe
Centre for Plasma Physics
Queen's University Belfast
Belfast BT7 1NN, UK

L. Bennie, Dr. J. A. Coulter, Prof. H. O. McCarthy
School of Pharmacy
Queen's University Belfast
Belfast BT7 1NN, UK

Dr. P. Quinn
Diamond Light Source
Harwell Science and Innovation Campus
Didcot OX11 0DE, UK

Prof. F. Currell
The Dalton Cumbrian Facility and the School of Chemistry
The University of Manchester
Manchester M13 9PL, UK
E-mail: frederick.currell@manchester.ac.uk

The ORCID identification number(s) for the author(s) of this article can be found under https://doi.org/10.1002/ppsc.201900140.

DOI: 10.1002/ppsc.201900140

microtoming can result in artifacts in positioning and heavy-metal stains used in sample preparation can be mistaken for small AuNPs.[18]

Recently developed imaging modalities have made significant advances in visualizing intracellular AuNPs in a less ambiguous manner. Video-enhanced color differential interference contrast (VECDIC) microscopy has been demonstrated as a means to directly image AuNPs in cells, doing so in a pseudo-3D manner.[19] Likewise, studies have implemented the Cytoviva microscopy technique which is also capable of directly imaging intracellular AuNPs.[20] Yet, a study which fully and accurately describes the 3D location of a proposed set of nuclear AuNPs is still lacking.

This study uses an imaging modality selected to circumvent these limitations, directly imaging the X-ray fluorescence (XRF) signal from elemental gold in whole cells. PC-3 human prostate cancer cells were cultured on silicone-nitride windows and treated with citrate-capped AuNPs functionalized with a modified RALA peptide (**Figure 1**a,b).[21] High-resolution dual angle-XRF microscopy was performed on cell samples (Figure 1c) and analysis of the resultant maps of elemental distribution across the imaged region yielded a 3D reconstruction of the nucleus and observed AuNPs (Figure 1d).

As such, reported herein is the first unambiguous evidence of individually resolved AuNPs within an intact cell nucleus, providing information on the individual nanoparticle level.

2. Results and Discussion

2.1. Detecting Gold Nanoparticles in Cells Using XRF

XRF measurements were performed on cell samples treated with RALA-AuNPs (see Sample Preparation, Experimental Section) using the I14 Hard X-Ray Nanoprobe beamline at the Diamond Light Source synchrotron facility. The samples were moved stepwise such that a 14 keV nanoscale X-ray beam scans over the desired region of the sample that is to be imaged.

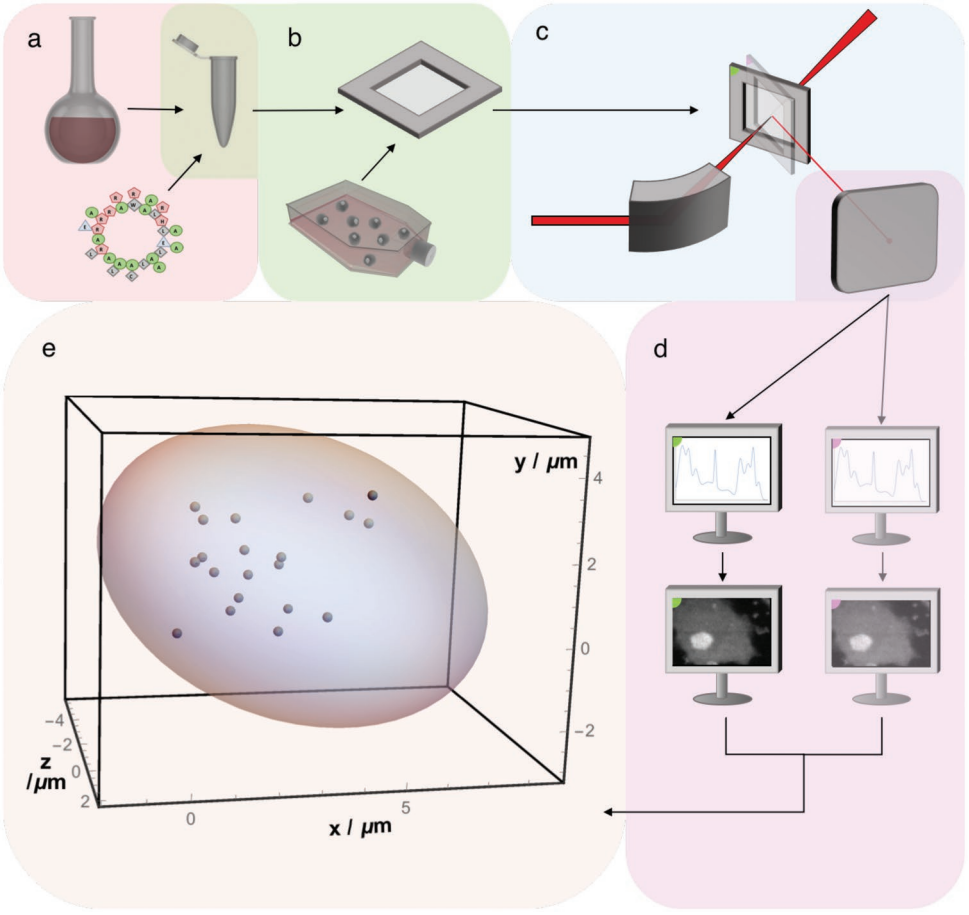

Figure 1. Demonstrating nuclear uptake of AuNPs through a 3D reconstruction of cancer cells imaged using dual-angle XRF. a) Citrate-capped AuNPs are modified with RALA peptide to impart nuclear targeting capabilities. b) The sample is prepared by culturing PC-3 human prostate cancer cells on a 200 nm thick silicon nitride membrane and treating with the RALA-AuNP preparation. c) A 14 keV X-ray nanobeam is focused on the sample and the sample is moved such that the beam scans the desired imaging region while a silicon drift detector collects the resultant photons. This is repeated with the sample having undergone a small rotation to achieve dual-angle XRF. d) The fluorescent spectra from each pixel are analyzed to create elemental maps at each angle. e) Analysis of these images yields a 3D reconstruction of the imaged cell's nucleus and the RALA-AuNP's within, shown as spheres with 3D error bars, demonstrating definitive evidence for the nuclear uptake of RALA-AuNP. The diameter of the AuNP spheres has been doubled for ease of viewing in this figure.

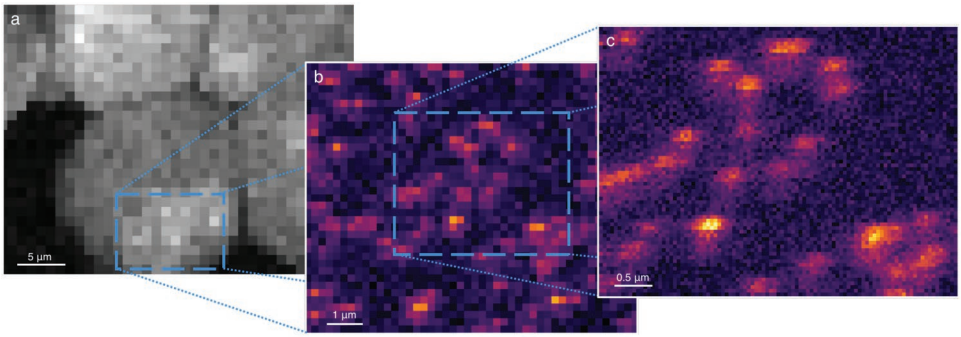

Figure 2. Multiscale XRF mapping of the distribution of elemental zinc and gold in cell of interest. a) Zinc distribution across chosen region showing the outline of the cell of interest and its nuclear region in low resolution (recorded using a sample step size of 1 µm) b) Gold distribution in mid resolution (sample step size of 200 nm) focusing on the nuclear region. c) Gold distribution using the system's highest resolution (sample step size of 50 nm) where individual AuNPs are clearly visible.

At each step characteristic photons were emitted by fluorescence and detected before being processed using the Dawn and PyMCA software packages to obtain pixel intensity information (see Imaging Procedure, Experimental Section).[22,23]

For each image collected and processed in this way a set of maps detailing the distribution of many different elements across the imaged region may be obtained. In this study, the elemental mapping of gold is of interest as this provides a truly direct route to detect the presence of AuNPs within the sample. Additionally, since it is known that the cell nucleus contains high levels of zinc due to the presence of zinc-finger proteins which are involved in gene regulation and nucleic acid binding,[24–26] the elemental distribution of zinc is also extracted to allow the boundary of the cell nucleus to be identified.

XRF can be a time-consuming process, as such initial large-area measurements were taken using a coarse step size of 1 µm, undersampling the region and thus creating maps of lower apparent resolution but in a relatively short time. Using an initially obtained map, the cell nucleus was then focused upon reducing the step size to generate a higher resolution map of this region of interest (**Figure 2**).

It is imperative to note that this result alone, where the AuNPs are seen to overlap with the location of the nucleus, should not be interpreted as evidence for successful nuclear uptake of the AuNP, as has been done in the past. XRF measurements provide 2D projection images, and as such cannot be used to extract the full 3D location of the image contents. With that being said, this study will demonstrate how simple extensions to this technique facilitate the extraction of a wealth of additional information regarding the imaged nanoparticles, including their precise 3D locations.

2.2. Characterization of RALA-AuNPs

RALA is a cell-penetrating peptide previously shown to enhance the in vitro and in vivo delivery of a variety of moieties such as nucleic acids and bisphosphonates.[27,28] The amphipathic nature of RALA with both hydrophobic and hydrophilic regions facilitates transport across cell membranes predominantly via clathrin-mediated endocytosis. One of the key differentiators with RALA lies in the secondary amphipathic structure.[21] When the pH drops to <5.5, the alpha-helicity of RALA increases facilitating endosomal escape and release of the cargo into the cytoplasm.

In this study, RALA-AuNPs were created as described in RALA-AuNP Production, Experimental Section. The AuNPs were initially characterized using dynamic light scattering (DLS) before and after functionalization with the RALA peptide, the results of which are shown in **Table 1**.

TEM images of the AuNPs before and after functionalization with the RALA peptide were also taken and used to measure the size of the gold core, as shown in the histogram in **Figure 3**. From these the average diameter of the AuNP core was determined to be 14.7 ± 1.7 nm, showing agreement with the value obtained via DLS.

Delving deeper, the measured AuNP diameters from TEM were used to calculate the typical distribution in volume of single AuNP cores. This volume is proportional to the number of gold atoms present in a given AuNP core, as is the intensity of the gold signal generated by the XRF process. As such, the distributions for AuNP volume, as per TEM, and for AuNP signal, as per XRF, ought to match when dealing with isolated, single nanoparticles.

To compare these distributions, the AuNP volume data from TEM are scaled between 0 and 1, as shown in blue in Figure 3. Cells treated with RALA-AuNPs were imaged using the XRF system's highest resolution and the gold signal strength of a sample of 53 nanoparticles was extracted. This signal was linearly scaled. As the polydispersity index (PDI) indicated, not all RALA-AuNPs observed in this study will be monodispersed and clearly resolved. As such, the XRF signal value at which to scale to 1 was left free to vary such that the best fit in the single AuNP regime may be found, shown in orange in Figure 3.

Table 1. Results of DLS characterization. DLS measurements were taken from AuNP samples before and after functionalization with the RALA peptide and presented are the obtained hydrodynamic radius, polydispersity index, and zeta potential for each.

	AuNP only	RALA-AuNP
Diameter [nm]	15.49 ± 2.6	65.31 ± 3.95
PDI	0.31± 0.03	0.35 ± 0.04
Zeta potential [mV]	−23.7 ± 11.3	17.55 ± 1.79

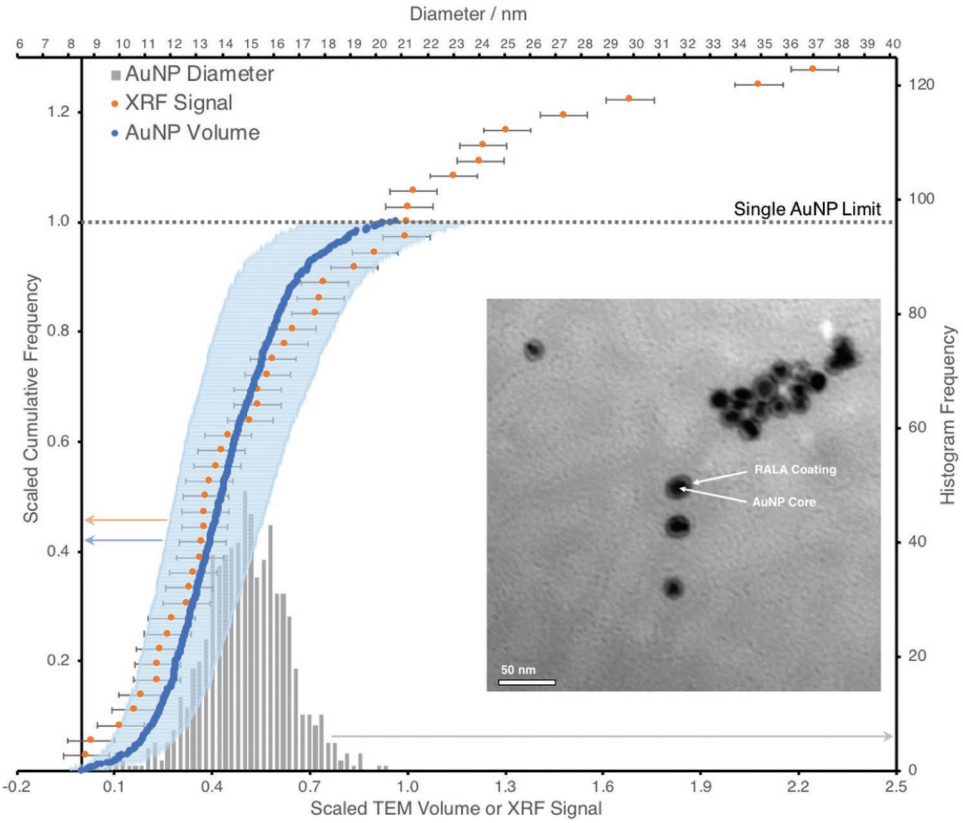

Figure 3. Characterization of the RALA-AuNPs. Shown in the inset image is a typical TEM image of the RALA-AuNPs post-functionalization. The size of the AuNP core was determined using TEM images of AuNPs pre-functionalization, shown in gray on the secondary axis is the histogram of measured core diameter. From this the distribution of AuNP volume was determined, shown as a cumulative frequency plot for the population sampled in blue. The distribution of measured gold signal intensity, generated by XRF imaging, for a sample of candidate monodispersed RALA-AuNPs, shown in orange, was fitted to this distribution to determine the maximum XRF signal for a single RALA-AuNP. All errors shown are representative of one standard deviation.

Through this process it was found that of the nanoparticles observed in the cell samples 68% of the population were monodispersed. A fraction of the remainder of the population may also be monodispersed but with a proximity below the image resolution limit. This finding shows strong agreement with the PDI data in Table 1, which found 65 ± 4% of the nanoparticles in stock RALA-AuNP preparation to be monodispersed, highlighting the robustness of the single AuNP XRF signal limit predicted here. The validity of this result is reinforced further still by the fact that the predicted single AuNP limit is just above twice the smallest measured AuNP signal, that is, the likely lower limit on signal for an AuNP doublet. It should also be noted that the nanoparticles shown in Figure 3 appear more agglomerated due to the dehydration step required for TEM imaging.

2.3. 3D Cell Reconstruction from Dual-Angle XRF

In order to facilitate the extraction of 3D information from the obtained XRF images, the sample regions shown in Figure 2 were imaged again, but with the sample having undergone a rotation of 10° about an axis perpendicular to the beam. By considering the distance between two objects in an image at one angle, $\Delta x_{\theta 1}$, and comparing with the new distance between those objects at the second angle, $\Delta x_{\theta 2}$, it is possible to deduce the relative depth of one object to the other, ΔZ, as shown in Equation (1) (Figure S1, Supporting Information)

$$\Delta Z = \frac{\Delta x_{\theta 1}}{\tan\theta} - \frac{\Delta x_{\theta 2}}{\sin\theta} \tag{1}$$

To analyze the gold elemental distribution maps in this manner, a custom 2D Gaussian fitter was written in Mathematica (see Gaussian Fitter, Experimental Section) for the purpose of determining the x-y centroid for each RALA-AuNP observed. Fitting was performed on the high and mid-resolution gold maps (Figure 2b,c) and their counterparts obtained after rotation allowing ΔZ values for each observed nanoparticle to be calculated relative to an arbitrarily chosen z-axis origin. In the case of the high-resolution images, errors arising from the Gaussian fitting process and rotational angle were propagated through the analysis chain to obtain error bars for ΔZ. The mid-resolution data set requires a slightly more detailed approach to error propagation as is described in Note S2 (Supporting Information).

To determine the 3D position of the nucleus and cell membrane, a slightly different approach was taken since

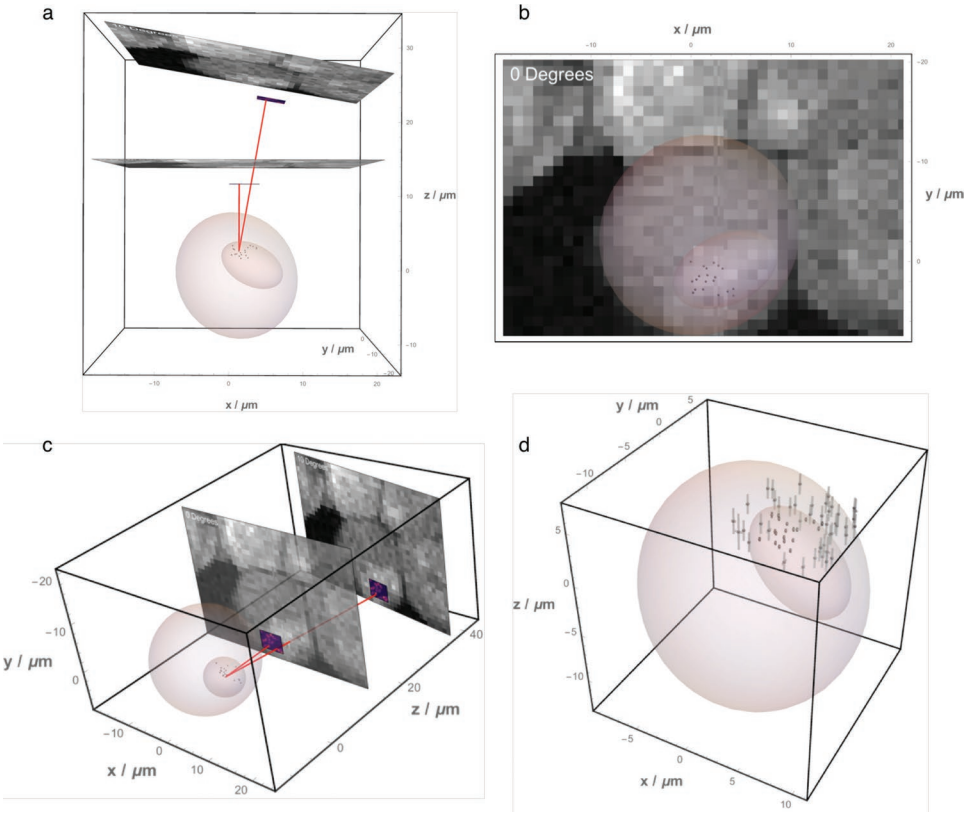

Figure 4. 3D reconstruction of cell membrane, nucleus, and observed AuNPs. a) Top-down view of a to-scale model showing the graphical reconstruction of cell and AuNPs and the dual-angle gold and zinc elemental maps from which it was derived. The red guidelines highlight a single AuNP observed in both images. b) Demonstrating the alignment of the 3D cell and nucleus model with the 0° zinc map. c) Side view of whole system. d) A blow-up image of the same reconstruction, but also showing the AuNPs observed using mid resolution in addition to their high-resolution counterparts. Clear evidence of nuclear uptake of said AuNPs is demonstrated in addition to many cellular and a few extracellular AuNPs being recorded. Nanoparticle width has been doubled to aid viewing.

these are single, continuous objects rather than multiple isolated objects as was the case with the AuNPs. A MATLAB script was written to fit the cell and nuclear boundaries, at both angles, to 2D ellipses (see Nucleus and Cell Outlining, Experimental Section). By determining the centroid and foci of the ellipses at both angles and treating them as point objects, as with the AuNP analysis, the z-position of these points were calculated relative to the predefined z origin. These data points were then used to construct ellipsoids of the cell and nucleus (see Graphical Reconstruction, Experimental Section).

Expanding upon this a 3D reconstruction combining the AuNP data with the cell and nucleus outlines was generated (**Figure 4**). Investigating the AuNPs observed in high resolution over the nuclear region (Figure 2c) this reconstruction reveals that not only have they clearly been endocytosed by the cell but also additionally 95% of this sample are unambiguously within the bounds of the nucleus (Figure 4a–c). This can be seen clearly by viewing Video S4 (Supporting Information) where the viewpoint spans around the cell of interest. Furthermore, inclusion of the AuNPs imaged in mid resolution across a wider field (Figure 2b) reveals all stages of the uptake pathway with nanoparticles being observed extracellularly, in the cytoplasm and within the nucleus (Figure 4d).

2.4. Validity of Nuclear Uptake

To make the claim that the AuNPs are definitely imaged inside a cell nucleus, it is necessary to ensure that this result is reliable.

First, consider the nucleus. The nuclear ellipsoid presented in Figure 4 is generated from a minimum case scenario. The 2D nuclear ellipses which give rise to the ellipsoid are fitted to pixels with a zinc XRF signal strength two standard deviations above the mean cytoplasmic response (Nucleus and Cell Outline, Experimental Section). As such, the reconstructed nucleus shown is a highly conservative estimation of the true nuclear volume. This is intentional to ensure any object observed within the reconstructed nucleus can be reliably demonstrated to have undergone nuclear uptake rather than association with the nuclear membrane. Furthermore, if the nuclear outlining procedure is relaxed slightly an analogous result is still achieved highlighting that this is not simply an ambiguous result (Figure S3, Supporting Information).

Consider then the accuracy of the location of the AuNPs. The diameter of the gold core of the RALA-AuNP is ≈15 nm, however under imaging in high resolution (Figure 2c) the nanoparticles appear to have a much larger size of 332 ± 82 nm at full width at half maximum (FWHM) when performing a 2D Gaussian fit. This observed FWHM is a convolution of several

factors including X-ray beam width, translator step reproducibility, and nanoparticle size. Gaussian fitting for each nanoparticle region has allowed the extraction of each AuNP centroid to an accuracy less than the 50 nm step size. As such, this gives rise to the relatively small error bars associated with AuNPs imaged in high resolution, placing 95% of them well within the nuclear boundary to a high degree of accuracy.

Additionally, it should be noted that this 95% rate of nuclear uptake is not representative of the entire population. Rather this is indicative of the nuclear region being specifically selected from the low resolution, 200 nm step size image (Figure 2a) possibly leading to a disproportionately high number of AuNPs observed inside the nucleus. This becomes apparent when including the nanoparticles observed in mid resolution which, while still capturing the nuclear region, were observed over a greater cellular area. As such, the percentage of AuNPs observed inside the nucleus drops to 45 ± 8%, a value which, while indeed closer to the global nuclear uptake percentage, should still be considered as disproportionately large due to the selection of the nucleus as the imaging region.

One interesting facet of the data shown in Figure 4 is that it appears few AuNPs occupy positions far into the negative *z*-axis volume of the cell. It is known that during culturing when cells adhere to the mounting surface their shape can deform slightly, being pulled broader and flatter, into a more "fried egg"-like shape.[29,30] When the gold was added to the cells they were already resident on the silicone-nitride window. Hence, the most direct route into the nucleus, both in terms of media access to the cell membrane and trafficking through the cytoplasm, would be from the top of the cell as observed.

2.5. The Significance of Observed Nuclear Uptake

As previously discussed, a direct measurement of the unequivocal uptake of AuNPs into the cell nucleus has not been reported in the field of nanomedicine, yet is highly important in evidencing the possible benefits of a given AuNP preparation. To illustrate this, we pick a specific application domain—the radiosensitization due to enhanced dose deposition around nanoparticles. While this application domain has been chosen because it is amenable to quantified calculation with the relevant computational machinery being at hand,[31] this finding illustrates the importance for any causal effect expected to be local to the nanoparticles. In fact, the dose enhancement roughly falls off with the second inverse power of distance from the nanoparticle, that is, d^{-2} where d is the distance between the nanoparticle and the site of effect. While it is not usual to think in these terms, a lot of other biological phenomena will fall off more rapidly (i.e., be more local). In these cases, the effect of penetration into the nucleus will be greater still.

The dominant physical effect giving rise to AuNP radiosensitization is the production of low-energy, short-range Auger electrons which cause dense ionization, and thus huge doses, for several hundred nanometers around the AuNP surface.[32] As such, the exact intracellular location of an AuNP is hugely important in determining the amount of nuclear DNA damage induced upon irradiation; AuNPs which fail to localize with the nuclear membrane, or ideally undergo uptake into the nucleus, will provide much greater DNA damage by the short-range low-energy electrons produced. Within this study we have demonstrated a definitive method by which to show that the RALA-AuNP preparation used has been taken up in the nucleus.

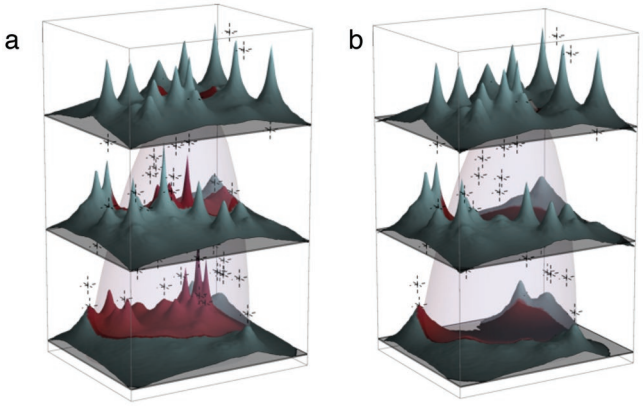

Figure 5. The dose-enhancement distribution arising from the presence of RALA-AuNPs in and around the nucleus during irradiation. A portion of the nuclear ellipsoid is shown along with nearby RALA-AuNPs observed in this study, each located at the intersection of the dashed lines. Three planes through the nucleus are chosen and the average dose increase due to the presence of the NPs across the plane is shown in 3D on a logarithmic vertical scale, the blue region denoting outside of nucleus and the red inside. The vertical aspect ratio in these figures is 3 (i.e., *z*-direction coordinates, vertical in the figures, were all multiplied by 3 for graphical purposes alone). a) The dose distribution with all nanoparticles included is shown. b) The nanoparticles with a probability greater than 50% of being inside the nucleus have been excluded. As expected, the NPs found to be inside the nucleus have a very significant effect on the dose enhancement inside the nucleus. The full dynamic range in dose enhancement observed is somewhat disguised by the logarithmic scale being approximately five orders of magnitude, with the highest dose enhancement in panel (a) being a factor of 69 000 greater than the lowest enhancement shown in the same panel.

Moreover, monodispersion within the nucleus would be the ideal distribution for maximizing DNA damage as this represents multiple sites where nuclear DNA damaging events have an opportunity to occur. Based on the RALA-AuNP characterization analysis, detailed previously in Figure 3, the nanoparticles imaged in high resolution were compared to the predicted XRF signal limit for a single, isolated nanoparticle. It was found that 79% of the RALA-AuNPs internalized by the nucleus had XRF responses lower than this limit and as such are indeed predicted to be monodispersed nanoparticles, once more showing how this technique can in new ways shed light on the potential benefits of nanoparticle-based treatments to patients.

To further illustrate the significance of these findings, a model was created to show the predicted dose enhancement that would arise during irradiation from this set of AuNPs in the real distribution in and around the nucleus as determined by this study (**Figure 5**). Recalling that the dose enhancement is being shown on a logarithmic intensity scale, this figure illustrates the significance of AuNP uptake into the nucleus. Removing from the simulation those nanoparticles which are in the nucleus results in a very significant depression in the dose enhancement to the nucleus.

The importance of nuclear uptake is clear from this model, RALA-AuNPs within the nucleus lead to huge nuclear dose

enhancements and hence much greater damage to the nuclear DNA. But further to this it can be seen that nuclear dose enhancements of this magnitude are not possible from extranuclear RALA-AuNPs alone, the effect is too short range. In order to gain a significant increase in damage to DNA, nuclear uptake of the nanoparticle is required. The technique of dual-angle XRF presented here has the potential to facilitate many future studies. Analogous experiments comparing and contrasting the uptake and localization of other functionalized nanoparticles could be carried out. The success of drug delivery systems which seek to target specific organelles could be assessed using this method.

3. Conclusion

In progressing the use of AuNP-enhanced radiotherapy to the clinic having a detailed knowledge of the uptake dynamics of AuNPs in cells is of great importance, with the degree of beneficial dose enhancement being highly dependent on the location of the AuNP within the cell. Historically many studies report cellular or nuclear uptake of nanoparticles using techniques which either assume knowledge of the depth of image contents or only provide an indirect and therefore not fully reliable measurement. Here, we have presented results showing the precise 3D location of AuNPs within the cell, reporting the first unambiguous evidence of the nuclear uptake of monodispersed AuNPs in a whole cell.

4. Experimental Section

Sample Preparation: PC-3 human prostate cancer cells (American Type Culture Collection, UK) were maintained in monolayers in a RPMI 1640 medium (Gibco, UK) which was supplemented with 10% fetal bovine serum (FBS). The cells were subcultured at 70–90% confluency, using 4 mL phosphate buffered saline solution to remove excess FBS. 0.05% trypsin (Gibco, UK) was added until full detachment of cells was achieved before being neutralized using an equal volume of complete medium and centrifuged at 50 *g* before resuspension to single cells.

The cells were then seeded onto 200 nm thick silicon nitride membrane windows (Norcada Inc.); the material holding the cell samples must undergo minimal interaction with the X-ray beam in order to perform XRF measurements. The cells were incubated for 24 h before treatment with a 25 μg mL^{-1} solution of RALA-AuNP. After a further 6 h the samples were fixed and dried.

Imaging Procedure: The Diamond Light Source synchrotron provides the I14 Hard X-Ray Nanoprobe beamline with a beam of X-rays being focused using nanofocusing KB mirrors, which can be adjusted over an energy range of 5–23 keV. For this study, a 14 keV X-ray energy was selected, allowing the L-α electronic transition of gold at 9.7 keV and the K-α transition of zinc at 8.6 keV to be probed.

XRF was performed using step sizes of the sample of 1 μm, 200 nm, and 50 nm in two directions perpendicular to the beam, the same step size being used for both directions in each raster scan. This was done with the same X-ray optics setup so the 1 μm step represents significant undersampling and was used for an initial survey. The 200 nm step size is close to the measured FWHM of XRF AuNP features of 332 ± 82 nm. While scans at this step size can be sure to show all of the nanoparticles in the field of view, using the even smaller step size of 50 nm gives rise to significant oversampling which in turn facilitates a smaller (subresolution) determination of the centroids of features observed.

The collected fluorescent photons were detected by a four-element silicon drift detector with a solid collection angle of 0.6–0.8 sr, operating 1.5 Mcps per channel. The PyMCA and DAWN software packages were used to perform analysis on the obtained fluorescent spectra by isolating the relevant peaks and converting to elemental intensity on a pixel-by-pixel basis, thereby generating elemental maps.[22,23]

RALA-AuNP Production: Aqueous AuNPs were created using the Turkevich method.[33] 400 mL of 0.01 w/v% gold(III) chloride hydrate solution (Sigma, UK) was added to a round bottomed flask and heated under reflux. Once boiling 9 mL of 1 w/v% sodium citrate (Sigma, UK) was added to the flask, it was heated for a further hour with stirring. The heat was then removed and the solution left to cool overnight with constant stirring before being reduced to a stock concentration of 33 μg mL^{-1} via centrifugation.

RALA peptide (Biomatik Corp., USA) was stored at −20 °C until resuspended in DNase/RNase-free water (Lifetech, UK) at 5.8 μg μL^{-1}. The RALA and AuNP solutions were combined, thoroughly pipetting to ensure the reagents were well mixed, to make a 50 μL volume containing 25 μg of peptide and incubated for 30 min at room temperature.

2D Gaussian Fitting Process for Gold Elemental Maps: For each gold elemental map obtained, ImageJ was used to select and crop a small "patch" around each observed AuNP, while also recording the coordinates defining where each patch is located with respect to its original, larger image. These patches were read by a Mathematica script which fitted each data set to a 2D Gaussian function, allowing the extraction of the centroid for each AuNP imaged.

In some cases where two AuNPs were observed in close proximity, making them difficult to individually analyze, it was necessary to use a double-Gaussian fitter to obtain accurate centroid positions.

Code available upon request from the author.

Nucleus and Cell Outline: A Matlab script was created with the general purpose of fitting an ellipse to candidate cell or nucleus pixels using the in-built "regionprops" function, thereby outlining the cell and nuclear membranes. This script outputs the coordinates of the ellipse's centroid, the size of its major and minor axis, and its orientation.

To isolate pixels of the cell of interest, ImageJ was used. A lower threshold on pixel intensity was increased until all pixels clearly in the extracellular region were removed. In a case such as Figure 2a where there are neighboring cells close to the cell of interest, this does not define a clear outline for the entire cell. It was necessary to perform the additional step of manually inspecting the pixel values and cropping the cell outline in accordance to the location of the minima between the two cells. The pixels within this cropped cell outline were then passed to the Matlab script for fitting.

In order to avoid a biased selection of nuclear pixels in Figure 2a, a sample of the upper half of the cell, clearly not containing nuclear pixels, was analyzed in ImageJ. The mean and standard deviation of this sample is therefore representative of the cytoplasmic zinc response. In order to be certain that no cytoplasmic pixels were taken into the nuclear fitting process, a threshold on pixel intensity was set 2σ above the mean of the cytoplasmic zinc response. Figure S4 (Supporting Information) shows the importance of this high threshold, reducing it to 1.5σ still shows good agreement with the obtained result but reducing to 1σ leads to the incorporation of stray cytoplasmic pixels and an erroneous result.

Code available upon request from the author.

Graphical Reconstruction: To reconstruct a 3D ellipsoid from two 2D ellipses, the parameters obtained from the ellipse fitting process at both angles are processed using a Mathematica script. The foci of the ellipses are determined as $\sqrt{a^2-b^2}$ where *a* and *b* are the semimajor axis and the semiminor axis, respectively. Depth analysis is performed as described by Equation (1) on the centroid and foci to infer their 3D positions. In this manner, the orientation of the ellipsoid in 3D space is obtained. The size of the ellipsoid is then determined from an average of the *a* and *b* parameters of the ellipses that produce it.

This process does rely on two assumptions. First, when the ellipsoid is reconstructed it is assumed that one is dealing with a spheroid, that is to say, an ellipse where two of the axes are equal in magnitude, in this case having the third axis equal to the average *b* parameter. Although this

is not entirely accurate as it is known that cells and nuclei are somewhat amorphous, it is however believed to be a good approximation.

Second, the average of the *a* and *b* parameters of the observed ellipses are equivalent to the *a* and *b* parameters of the ellipsoid. This assumption is not entirely accurate, unless the ellipsoid was oriented such that it was close to casting the maximum projection "shadow" at both angles of observation then this equivalency is not strictly true. However, the ellipsoid reconstructed will be contained entirely within the true volume of the real ellipsoid. For the purpose of this study, nuclear uptake is shown and therefore this assumption actually only goes further in assuring the validity of the claim; the nucleus reconstructed is within the bounds of the true nucleus but may in fact be slightly smaller in volume.

The same Mathematica code was then used to combine the dataset describing the 3D location of the RALA-AuNPs with the nucleus and cell ellipsoids to give a full reconstruction of the obtained data.

Code available upon request from the author.

Dose Deposition Simulation: The dose enhancement due to the Au-NPs was calculated using a multiscale Monte Carlo method.[31] Using Topas,[34] a clinical linac spectrum,[35] after transport through 3 cm of soft tissue, was further transported through a single nanoparticle (including its coating) with the outgoing phase space of all particles interacting with the nanoparticle or its coating being captured. These outgoing particles were then transported through a large volume of water with the dose deposition being scored in spherical symmetry to give the required radial dose distribution (RDD). The dose distributions shown in Figure 5 were determined by superposition of many of these RDDs, treating them as spherical kernel functions centered on each nanoparticle. Where it was believed there were two unresolved nanoparticles, a double weighting was applied. Two such simulations were conducted, one with all the nanoparticles being used, one with only those outside the nucleus being used. This then gives the average dose enhancement due to the presence of the nanoparticles.

Supporting Information

Supporting Information is available from the Wiley Online Library or from the author.

Acknowledgements

The authors thank and acknowledges financial support from the Department for Employment and Learning Northern Ireland and from the Centre for Advanced Interdisciplinary Radiation Research (CAIRR). The authors also acknowledge Diamond Light Source for time on the I14 beamline under proposals SP16931 and SP17932. Thanks to C. Figueira and K. Holsgrove for their help with TEM measurements. Also, thanks to the team on the I14 beamline for all their assistance in running these experiments and for their continued support.

Conflict of Interest

The authors declare no conflict of interest.

Keywords

gold nanoparticles, nanomedicine, nuclear uptake, X-ray fluorescence, X-ray microscopy

Received: April 2, 2019
Revised: June 18, 2019
Published online: July 30, 2019

[1] F. Currell, B. Villagomez-Bernabe, in *Gold Nanoparticles Physics, Chemistry and Biology* (Eds: O. Pluchery, C. Louis), World Scientific, Singapore **2017**, pp. 509–536.
[2] B. D. Chithrani, A. A. Ghazani, W. C. W. Chan, *Nano Lett.* **2006**, *6*, 662.
[3] R. A. Sperling, P. Rivera Gil, F. Zhang, M. Zanella, W. J. Parak, *Chem. Soc. Rev.* **2008**, *37*, 1896.
[4] L. Wang, Y. Liu, W. Li, X. Jiang, Y. Ji, X. Wu, L. Xu, Y. Qiu, K. Zhao, T. Wei, Y. Li, Y. Zhao, C. Chen, *Nano Lett.* **2011**, *11*, 772.
[5] J. F. Hainfeld, D. N. Slatkin, H. M. Smilowitz, *Phys. Med. Biol.* **2004**, *49*, N309.
[6] G. Han, C. C. You, B. J. Kim, R. S. Turingan, N. S. Forbes, C. T. Martin, V. M. Rotello, *Angew. Chem., Int. Ed.* **2006**, *45*, 3165.
[7] P. Ghosh, G. Han, M. De, C. K. Kim, V. M. Rotello, *Adv. Drug Delivery Rev.* **2008**, *60*, 1307.
[8] B. Kang, M. A. Mackey, M. A. El-Sayed, *J. Am. Chem. Soc.* **2010**, *132*, 1517.
[9] D. H. M. Dam, J. H. Lee, P. N. Sisco, D. T. Co, M. Zhang, M. R. Wasielewski, T. W. Odom, *ACS Nano* **2012**, *6*, 3318.
[10] S. Huo, S. Jin, X. Xue, K. Yang, A. Kumar, P. C. Wang, J. Zhang, Z. Hu, X. Liang, *ACS Nano* **2014**, *8*, 5852.
[11] P. Nativo, I. A. Prior, M. Brust, *ACS Nano* **2008**, *2*, 1639.
[12] L. Singh, R. Parboosing, H. G. Kruger, G. E. M. Maguire, T. Govender, *Adv. Nat. Sci.: Nanosci. Nanotechnol.* **2016**, *7*, 045013.
[13] S. W. Botchway, J. A. Coulter, F. J. Currell, *Br. J. Radiol.* **2015**, *88*, 20150170.
[14] R. Hong, G. Han, J. M. Fernández, B. J. Kim, N. S. Forbes, V. M. Rotello, *J. Am. Chem. Soc.* **2006**, *128*, 1078.
[15] H. He, C. Xie, J. Ren, *Exposure* **2008**, *80*, 1.
[16] W. Jiang, B. Y. S. Kim, J. T. Rutka, W. C. W. Chan, *Nat. Nanotechnol.* **2008**, *3*, 145.
[17] Z. L. Wang, *J. Phys. Chem. B* **2000**, *104*, 1153.
[18] A. M. Schrand, J. J. Schlager, L. Dai, S. M. Hussain, *Nat. Protoc.* **2010**, *5*, 744.
[19] A. G. Tkachenko, H. Xie, Y. Liu, D. Coleman, J. Ryan, W. R. Glomm, M. K. Shipton, S. Franzen, D. L. Feldheim, *Bioconjugate Chem.* **2004**, *15*, 482.
[20] C. Yang, J. Uertz, D. Yohan, B. D. Chithrani, *Nanoscale* **2014**, *6*, 12026.
[21] H. O. McCarthy, J. McCaffrey, C. M. Mccrudden, A. Zholobenko, A. A. Ali, J. W. McBride, A. S. Massey, S. Pentlavalli, K. H. Chen, G. Cole, S. P. Loughran, N. J. Dunne, R. F. Donnelly, V. L. Kett, T. Robson, *J. Controlled Release* **2014**, *189*, 141.
[22] M. Basham, J. Filik, M. T. Wharmby, P. C. Y. Chang, B. El Kassaby, M. Gerring, J. Aishima, K. Levik, B. C. A. Pulford, I. Sikharulidze, D. Sneddon, M. Webber, S. S. Dhesi, F. Maccherozzi, O. Svensson, S. Brockhauser, G. Náray, A. W. Ashton, *J. Synchrotron Radiat.* **2015**, *22*, 853.
[23] V. A. Solé, E. Papillon, M. Cotte, P. Walter, J. Susini, *Spectrochim. Acta, Part B* **2007**, *62*, 63.
[24] Q. Lu, H. Haragopal, K. G. Slepchenko, C. Stork, Y. V. Li, *Int. J. Physiol. Pathophysiol. Pharmacol.* **2016**, *8*, 35.
[25] J. M. Berg, H. A. Godwin, *Annu. Rev. Biophys. Biomol. Struct.* **1997**, *26*, 357.
[26] B. S. Twining, S. B. Baines, N. S. Fisher, J. Maser, S. Vogt, C. Jacobsen, A. Tovar-Sanchez, S. A. Sañudo-Wilhelmy, *Anal. Chem.* **2003**, *75*, 3806.
[27] A. S. Massey, S. Pentlavalli, R. Cunningham, C. M. McCrudden, E. M. McErlean, P. Redpath, A. A. Ali, S. Annett, J. W. McBride, J. McCaffrey, T. Robson, M. E. Migaud, H. O. McCarthy, *Mol. Pharm.* **2016**, *13*, 1217.
[28] R. Bennett, A. Yakkundi, H. D. McKeen, L. McClements, T. J. McKeogh, C. M. McCrudden, K. Arthur, T. Robson, H. O. McCarthy, *Nanomedicine* **2015**, *10*, 2989.

[29] T. Yeung, P. C. Georges, L. A. Flanagan, B. Marg, M. Ortiz, M. Funaki, N. Zahir, W. Ming, V. Weaver, P. A. Janmey, *Cell Motil. Cytoskeleton* **2005**, *60*, 24.
[30] C.-M. Lo, H.-B. Wang, M. Dembo, Y.-L. Wang, *Biophys. J.* **2000**, *79*, 144.
[31] B. Villagomez-Bernabe, F. J. Currell, *Sci. Rep.* **2019**, *9*, 8156.
[32] S. J. McMahon, W. B. Hyland, M. F. Muir, J. A. Coulter, S. Jain, K. T. Butterworth, G. Schettino, G. R. Dickson, A. R. Hounsell, J. M. O'Sullivan, K. M. Prise, D. G. Hirst, F. J. Currell, *Sci. Rep.* **2011**, *1*, 1.
[33] J. Turkevich, *Gold Bull.* **1985**, *18*, 125.
[34] J. Perl, J. Shin, B. Faddegon, H. Paganetti, *Med. Phys.* **2012**, *39*, 6818.
[35] R. Capote, "Phase-space database for external beam radiotherapy," https://www-nds.iaea.org/phsp/photon/Varian_TrueBeam_6MV/ (accessed: April 2018).